Diffractive Interactions: Experimental Summary

D.M. Jansen[a], M. Albrow[b] and R. Brugnera[c]

[a]Max–Planck–Institut für Kernphysik, Saupfercheckweg 1, 69117 Heidelberg, Germany

[b]Fermilab, P.O. Box 500, Batavia, IL 60510–0500, U.S.A.

[c]Dipartimento di Fisica dell' Università and INFN, Padova , Italy

Experimental results on diffraction, which were presented at the 7th International Workshop on Deep Inelastic Scattering and QCD (DIS99), are summarized.

1. Introduction

During the two days of parallel sessions at DIS99, there were 19 experimental talks about diffractive interactions on topics ranging from new measurements of $F_2^{D(3)}$ at HERA to the observation of double–gap events at the Tevatron. This paper summarizes the experimental results on diffraction which were presented. The theoretical talks concerning diffractive interactions are summarized in the following contribution.

2. Inclusive Diffraction in DIS

M. Inuzuka presented the new ZEUS measurement of diffractive cross sections at very low Q^2 [1]. Using 1996 data obtained with their beam pipe calorimeter, ZEUS has measured $d\sigma/dM_X$ as a function of W in the range $0.220 < Q^2 < 0.700$ GeV^2 (Figure 1). Regge theory predicts that $d\sigma/dM_X \simeq W^{4\overline{\alpha}_{\mathbb{P}}-4}$ and a fit to the data yields an effective ($|t|$ averaged) pomeron intercept equal to: $\overline{\alpha}_{\mathbb{P}} = 1.113 \pm 0.026$ (stat) $^{+0.043}_{-0.062}$ (syst). This value is approximately 1σ larger than the soft pomeron intercept $\alpha_{\mathbb{P}}(0) \simeq 1.09$ determined by Donnachie, Landshoff and Cudell [2, 3]. Assuming $\alpha'_{\mathbb{P}} = 0.25$ GeV^{-2} and $|t| = 1/b$ with $b = 7.5$ GeV^{-2}, $\alpha_{\mathbb{P}}(0) = \overline{\alpha}_{\mathbb{P}} + 0.033$.

C. Royon presented the H1 preliminary measurement of $F_2^{D(3)}$ in the kinematic range $0.4 < Q^2 < 5$ GeV^2 and $0.001 < \beta < 0.65$ [4]. The low Q^2 data were obtained during 1995 when the interaction vertex was shifted by 70 cm. In
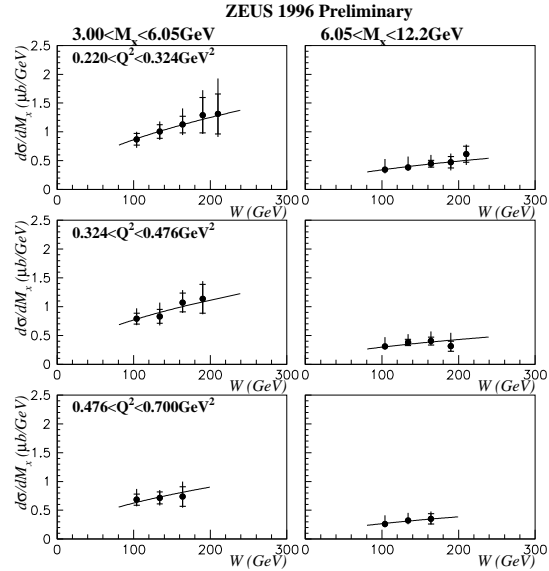

Figure 1. The differential cross section $d\sigma/dM_X$ as a function of W. The solid line shows the fit result for $d\sigma/dM_X \simeq W^{4\overline{\alpha}_{\mathbb{P}}-4}$.

Figure 2, the H1 measurement of $x_{\mathbb{P}} \cdot F_2^{D(3)}$ is compared to a phenomenological fit with diffractive ($\mathbb{P}$) and sub–leading ($\mathbb{R}$) exchange trajectories. The fitted pomeron intercept is consistent with the previous H1 measurement: $\alpha_{\mathbb{P}}(0) = 1.203 \pm 0.020$ (stat) ± 0.013 (syst) $^{+0.030}_{-0.035}$ (model) [5]. This value is significantly larger than the soft

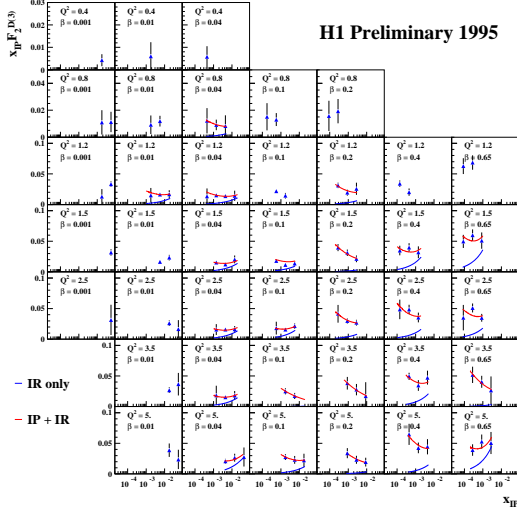Figure 2. $x_{\mathbb{P}} \cdot \mathrm{F}_2^{\mathrm{D}(3)}$ shown as a function of $x_{\mathbb{P}}$ in bins of Q^2 and β. The data are compared to a Regge based phenomenological fit.

Figure 3. Diffractive $D^{*\pm}$ cross sections $\mathrm{d}\sigma/\mathrm{d}p_T$ and $\mathrm{d}\sigma/\mathrm{d}\eta$ from the ZEUS collaboration compared to Monte Carlo predictions.
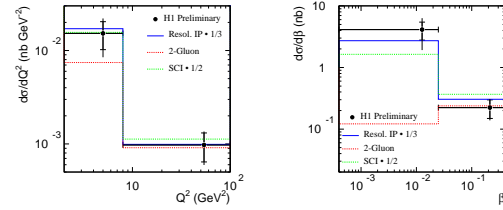
Figure 4. Diffractive $D^{*\pm}$ cross sections $\mathrm{d}\sigma/\mathrm{d}Q^2$ and $\mathrm{d}\sigma/\mathrm{d}\beta$ from the H1 collaboration compared to Monte Carlo predictions.

pomeron intercept. The H1 collaboration also presented their measurement of $\mathrm{F}_2^{\mathrm{D}(3)}$ in the high Q^2 range $200 < Q^2 < 800$ GeV^2. A QCD fit to the intermediate Q^2 data, with parton distributions for the pomeron and sub–leading reggeons which evolve according to the DGLAP [6] equations, gives a reasonable description of the high Q^2 data.

3. Hadronic Final State in Diffractive Interactions

The H1 collaboration has performed a NLO DGLAP analysis of their $\mathrm{F}_2^{\mathrm{D}(3)}$ measurement with $4.5 < Q^2 < 75$ GeV^2 and extracted diffractive parton distributions [5]. These partons distributions when incorporated into Monte Carlo programs give a good description of the hadronic final state in hard diffractive processes. As an example of this, F.P. Schilling presented the H1 measurements of diffractive dijet production in $ep \rightarrow eXY$ interactions with $M_Y < 1.6$ GeV and $|t| < 1$ GeV^2 [7]. The system X contains two jets each with $p_T > 5$ GeV. The POMPYT [8] and
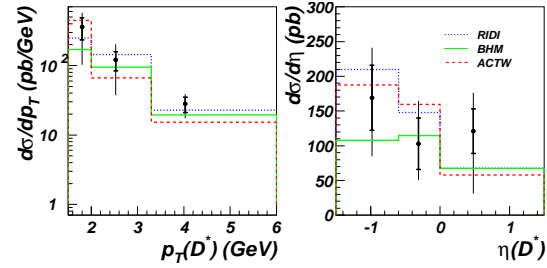
RAPGAP [9] Monte Carlo programs, with either a 'flat' or a 'peaked' gluon distribution, give good descriptions of the photoproduction and DIS data which were presented. Predictions, calculated using diffractive parton distributions which consist solely of quarks at the starting scale, underestimate the measured cross sections by factors varying between 3 and 6.

Diffractive $D^{*\pm}$ cross section measurements were presented by S. Hengstmann and J. Cole for the H1 and ZEUS collaborations respectively [10, 11]. Both experiments use the $D^{*+} \rightarrow (D^0 \rightarrow K^-\pi^+)\pi^+ + $(c.c.) decay mode whereas the ZEUS collaboration also uses the $D^{*+} \rightarrow (D^0 \rightarrow K^-\pi^+\pi^-\pi^+)\pi^+ + $(c.c.) decay mode. The cross section measurements for the two decay modes from ZEUS are in excellent agreement when interpolated to the same kinematic region and are in good agreement with Monte Carlo calculations.
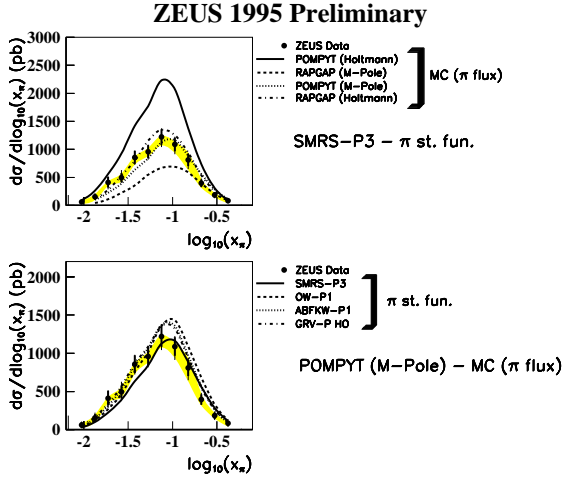
ZEUS 1995 Preliminary

Figure 5. The photoproduction cross section $d\sigma/d\log(x_\pi)$ compared to Monte Carlo calculations with various pion flux factors (top) and various pion parton distributions (bottom).

Figure 6. Average thrust $< T >$ and sphericity $< S >$ as a function of M_X for events tagged with a leading proton with $x_L > 0.95$.

The BHM [12] Monte Carlo prediction shown in Figure 3 is based on soft colour interactions, whereas in the RIDI [13] Monte Carlo diffractive charm production is proportional to the square of the gluon density in the proton. The ACTW [14] Monte Carlo is a resolved pomeron model with diffractive parton distributions which evolve according to the DGLAP [6] equations. The good agreement between data and model calculations shown in Figure 3 is in contradiction with the results presented by S. Hengstmann. Figure 4 shows that the H1 diffractive $D^{*\pm}$ cross sections are approximately a factor of 3 smaller than the prediction from a resolved pomeron model (RAP-GAP [9]) and a factor of 2 smaller than the prediction from a soft colour interactions model (AROMA [15]).

M. Khakzad presented the new ZEUS measurement of dijet cross sections associated with a leading neutron [16]. By requiring a leading neutron with $E_n > 400$ GeV and $\theta_n < 0.8$ mrad, π^+–exchange events are tagged. The fraction of the pion's momentum participating in the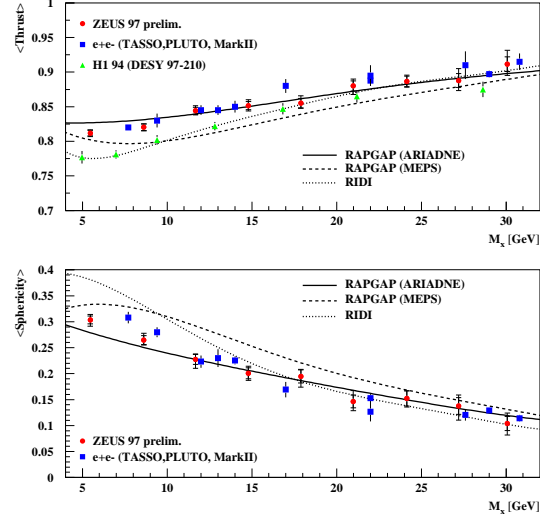 production of the two jets can be estimated using the final state variable $x_\pi = \sum_{jets} E_T^{jets} e^{\eta^{jet}}/2E_\pi$. The ZEUS measurement of $d\sigma/d\log(x_\pi)$, presented in Figure 5, shows that in the kinematic region of the measurement the x_π distribution has only a mild sensitivity to the pion's structure function. The Monte Carlo calculations have a larger sensitivity to differences in the pion flux.

M. Kapichine presented the H1 measurements of semi–inclusive cross sections in the kinematic region $2 \leq Q^2 \leq 50$ GeV^2, $6 \cdot 10^{-5} \leq x \leq 6 \cdot 10^{-3}$ and baryon $p_T \leq 200$ MeV [17]. The semi–inclusive cross sections are parameterized in terms of a leading baryon structure function, either $F_2^{LP(3)}$ or $F_2^{LN(3)}$, for protons or neutrons respectively. The leading baryon structure functions with $z > 0.7$ are reasonably well described by a Regge model of baryon production which considers the colour neutral exchanges of pions, pomerons and secondary reggeons. The semi–inclusive cross sections for leading neutrons can be described entirely by π^+ exchange whereas leading protons require π^0 and f_2 exchange contributions. The leading neutron data were used to estimate for the first time the structure function of the pion at small Bjorken–x.

Results on leading baryon production from ZEUS were presented by I. Gialas [18]. The x_L spectrum of leading protons with $p_T^2 < 0.5\text{GeV}^2$ is well described by a Regge model of leading baryon production whereas standard Monte Carlo programs, such as ARIADNE [19] and LEPTO [20], fail to describe the data. The ratio of events with a leading baryon and all DIS events is independent of x and Q^2 which supports the hypothesis of limiting fragmentation [21].

P. Markun presented results on the hadronic final state in diffractive DIS from ZEUS [22]. Figure 6 shows the average thrust and sphericity of diffractive events as a function of M_X for events tagged with a leading proton with $x_L > 0.95$. The analysis was performed in the $\gamma^*\mathbb{P}$ centre of mass system. The ZEUS measurements are compatible with the $\sqrt{s}$ dependence observed in e^+e^- events and are in fair agreement with the predictions from the RAPGAP [9] Monte Carlo implemented with ARIADNE [19] colour dipole fragmentation. The average thrust and sphericity measurements are independent of $x_{\mathbb{P}}$, Q^2 and W. Energy flow measurements in the $\gamma^*\mathbb{P}$ cms frame show that a two jet structure becomes increasingly pronounced as M_X increases.

B. Cox presented the H1 measurement of double diffractive dissociation at large $|t|$ in photoproduction [23]. The inclusive double dissociative process $\gamma p \to XY$ provides access to larger rapidity gaps than does the traditional gap–between–jets approach. This is advantageous since the BFKL cross section is expected to rise exponentially as a function of the rapidity separation [24]. In Figure 7 the differential cross section $d\sigma/dx_{\mathbb{P}}\,(\gamma\,p \to XY)$ is compared with the prediction from the HERWIG [25] Monte Carlo for all non colour–singlet exchange processes. A significant excess above the expectation from the standard photoproduction model is observed. The dashed line shows the HERWIG prediction with the LLA BFKL contribution added. Good agreement is observed in both normalization and shape.
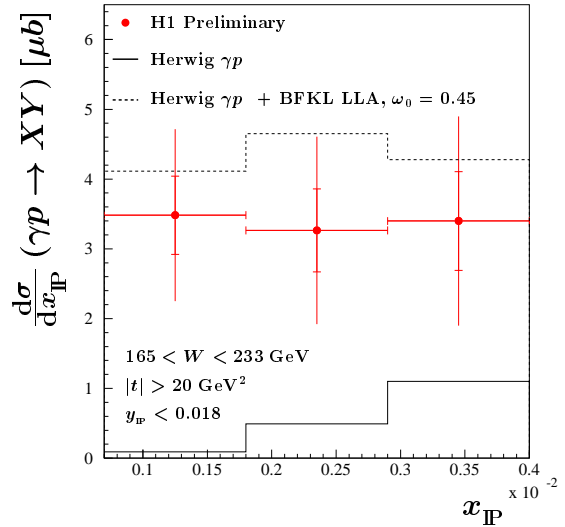

Figure 7. The differential cross section $d\sigma/dx_{\mathbb{P}}\,(\gamma\,p \to XY)$.

4. Diffractive Vector Meson Production

At DIS99 many new results on vector meson production were shown. B. Clerbaux presented H1 results on elastic electroproduction of ρ mesons in the kinematic region $1 < Q^2 < 60 \text{ GeV}^2$ and $30 < W < 140$ GeV [26]. Results on the shape of the $(\pi\pi)$ mass distribution were presented which indicate significant skewing at low Q^2, which gets smaller with increasing Q^2. No significant W or $|t|$ dependence of the skewing is observed. Measurements of the 15 elements of the ρ spin density matrix were also presented as a function of Q^2, W and $|t|$ (see Figure 8 for example). Except for a small but significant deviation from zero of the r_{00}^5 matrix element, s–channel helicity conservation (SCHC) is found to be a good approximation. The dominant helicity flip amplitude T_{01} is $(8 \pm 3)\%$ of the non–flip amplitudes. The W dependence of the measured $\gamma^*p \to \rho p$ cross sections, for six fixed values of Q^2 (Figure 9), suggests that the effective trajectory governing ρ electroproduction is larger than the soft pomeron intercept determined by Donnachie, Landshoff and Cudell [2, 3].
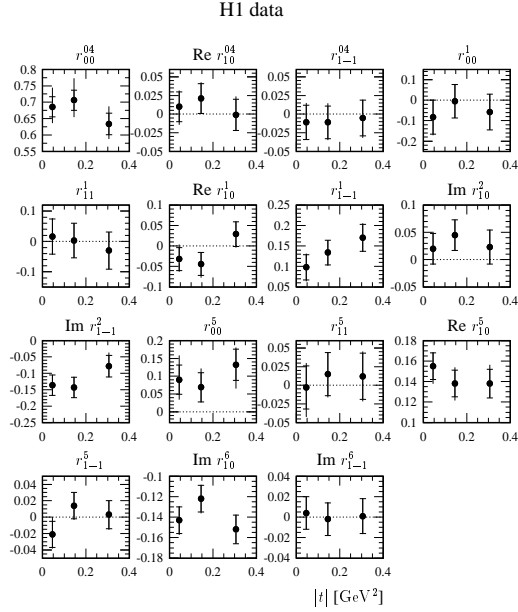
H1 data

Figure 8. The 15 spin density matrix elements for elastic electroproduction of ρ mesons as a function of $|t|$. The dashed lines indicate the expected null values in the case of SCHC.

Figure 9. The Q^2 dependence of $\alpha_{\mathbb{P}}(0)$ for elastic ρ electroproduction.

Preliminary results from H1 on proton dissociative ρ meson production were presented by A. Droutskoi [27]. Proton dissociative events are tagged by requiring activity in either the forward part ($\eta > 2.7$) of the LAr calorimeter, the forward muon detector or the proton remnant detector. An indication is observed for an increase in the ratio of proton dissociative to elastic ρ meson cross sections in the region $1.5 < Q^2 < 3$ GeV^2, in contrast with the approximately flat behavior of the ratio in the region $Q^2 > 3$ GeV^2. Results were also presented on the angular distributions characterizing the ρ meson production and decay.

New results on exclusive ω meson production from ZEUS were presented by A. Savin [28]. In the kinematic range $40 < W < 120$ GeV and $3 < Q^2 < 30$ GeV^2, $\sigma(\gamma^* p \to \omega p) \simeq W^{0.7}$ and $\sigma(\gamma^* p \to \omega p) \simeq 1/(Q^2 + M_\omega^2)^2$. These dependencies are consistent with those found for the ρ.

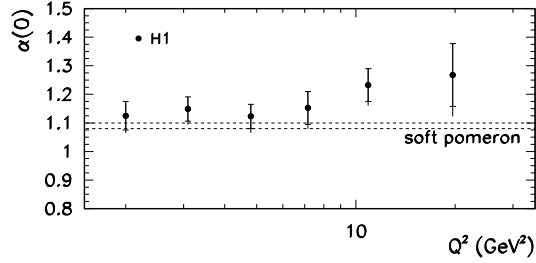The ratio of $\rho : \omega : \phi$ production, which is shown in Figure 10, is in good agreement at large Q^2 with the SU(3) prediction $9 : 1 : 2$. Exclusive cross sections, for the production of ρ, ϕ and ω vector mesons, are found to be proportional to W^δ where δ increases with Q^2. Results were also presented which show that SCHC is violated for exclusive ρ meson production in the low Q^2 range $0.25 < Q^2 < 0.85$ GeV^2.

J. Crittenden presented new results from the ZEUS collaboration on ρ^0 photoproduction at high momentum transfer $|t|$ [29]. Measurements of r_{00}^{04} (Figure 11), in the range $1 < |t| < 9$ GeV^2, were presented which show that the ρ^0 does not become dominantly longitudinally polarized at large values of $|t|$ [30, 31]. Evidence for a non–zero value of the double–flip amplitude r_{1-1}^{04} at large $|t|$ was also presented.

P. Merkel presented new H1 results on the elastic production of J/ψ and $\psi(2S)$ mesons in the kinematic region $2 < Q^2 < 80$ GeV^2 and $25 < W < 160$ GeV [32]. The dependence of the cross section $\sigma(\gamma^* p \to J/\psi p)$ on W is proportional to W^δ, with $\delta \simeq 1$ which has also been observed in photoproduction. The Q^2 dependence is proportional to $1/(Q^2 + m_{J/\psi}^2)^n$ with $n = 2.38 \pm 0.11$. The first evidence from HERA for the quasi–elastic production of $\psi(2S)$ in DIS was also reported. The ratio of cross sections for $\psi(2S)$ and J/ψ production increases as a function of Q^2.

Results on exclusive ρ^0 electroproduction from the HERMES collaboration were presented by

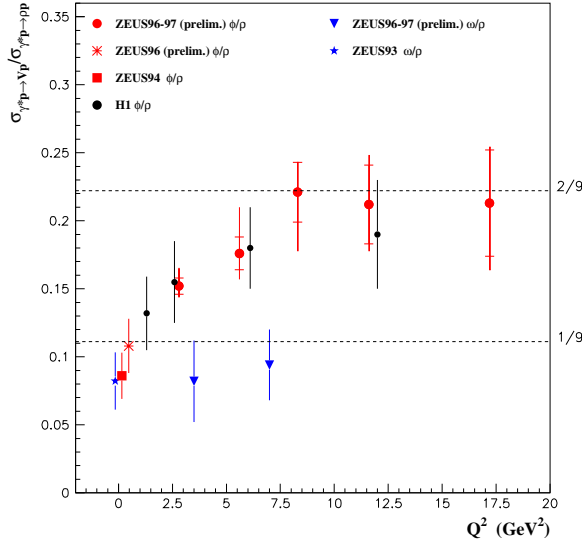Figure 10. The Q^2 dependence of vector meson cross section ratios.

Figure 11. The spin density matrix element r_{00}^{04} as a function of $|t|$ for ρ^0 photoproduction.

A. Borissov [33]. Using ^{1}H, ^{2}H, ^{3}He and ^{14}N targets, the ratio of cross sections per nucleon $\sigma_A/(A\sigma_H)$, known as the nuclear transparency, was found to decrease with increasing coherence length of quark–antiquark fluctuations of the virtual photon. An unperturbed virtual state with mass $M_{q\bar{q}}$ can travel a coherence length distance $l_c = 2\nu/(Q^2 + M_{q\bar{q}}^2)$ in the laboratory frame during its lifetime. The data presented showed clear evidence for the interaction of the quark–antiquark fluctuations with the nuclear medium.

5. Diffraction at the Tevatron and LEP Colliders

Results on hard diffraction from CDF were presented by K. Borras [34]. Using a sample of diffractive dijet events, with a recoil beam particle tagged with Roman Pot detectors, CDF has extracted the momentum fraction of the interacting parton in the pomeron using the formula $\beta = (E_T^{jet1}e^{-\eta^{jet1}} + E_T^{jet2}e^{-\eta^{jet2}})/2\xi P_{beam}$ where ξ is the momentum fraction of the beam particle taken by the pomeron. After subtracting
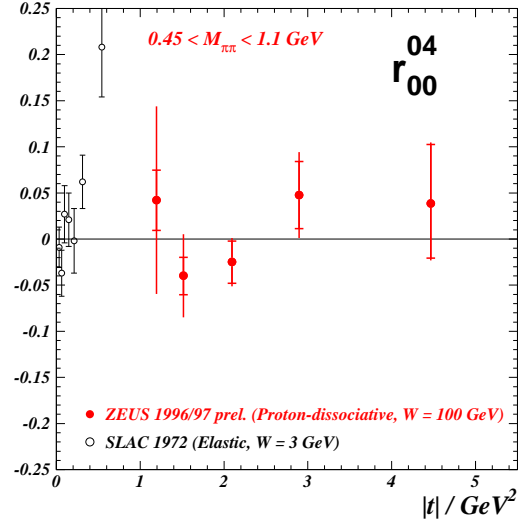
background contributions, such as non–diffractive dijet production with an accidental hit in the Roman Pot detectors and the contribution due to meson exchange, the data were compared to Monte Carlo simulations assuming various pomeron parton distributions and pomeron flux parametrizations. Figure 12 shows for three jet energy thresholds the ratio of the CDF diffractive dijet data and Monte Carlo predictions as a function of β. The Monte Carlo predictions were calculated with the H1 'peaked' gluon distribution [5] for the pomeron. The ratios are flat for $\beta > 0.2$ and approximately equal to 0.15. This result implies that the β distributions agree well with the shape of the H1 pomeron structure function but that there is a discrepancy between the data and the normalization of the standard pomeron flux. For $\beta > 0.2$, the shape and rate of the β distributions agree well with Monte Carlo predictions calculated with Goulianos's renormalized flux [35] and a flat gluon distribution, although an enhancement still exists in the $\beta < 0.2$ region.

K. Mauritz presented results on hard diffraction from D0 [36]. The fraction of single diffractive dijet events at $\sqrt{s} = 1800$ GeV and 630 GeV
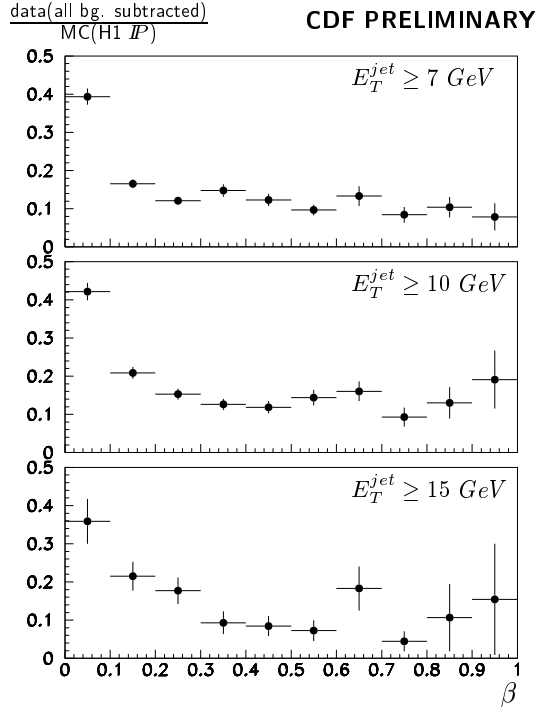
Figure 12. Ratio of CDF diffractive dijet data and Monte Carlo predictions as a function of β. The Monte Carlo predictions were calculated using the H1 'peaked' gluon distribution for the pomeron.

were compared to Monte Carlo predictions. Predictions calculated with hard or flat gluon distributions give rates which are higher than observed in the data. For example, the fraction of 1800 FWD Jet events observed in the data is $(0.64 \pm 0.05)\%$ compared to the hard and soft gluon predictions equal to $(2.1 \pm 0.3)\%$ and $(1.6 \pm 0.3)\%$ respectively. A comparison was also presented between the E_T spectra of the leading two jets in double–gap events and the E_T spectra observed in single diffractive and inclusive interactions. In spite of the decreasing effective centre of mass energies $(\sqrt{s}_{DG} < \sqrt{s}_{SD} < \sqrt{s}_{INC})$, Figure 13 shows that the E_T distributions are similar in shape which suggests a hard structure for the pomeron. A study of event characteristics shows that diffractive events are quieter, and contain thinner jets, than do non–diffractive events. The
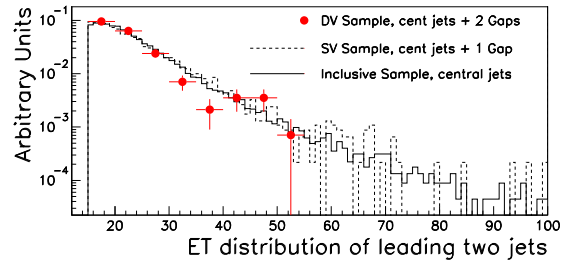

Figure 13. The E_T distributions of the leading two jets in double–gap, single diffractive and inclusive interactions from the D0 collaboration.

same conclusions have been reached by CDF.

H. Vogt presented L3 results on hadron production in $\gamma\gamma$ collisions at LEP [37]. Cross sections measurements with quasi–real photons (anti–tagged events where the scattered electrons are not detected) and with virtual photons (where both scattered electrons are detected in small angle calorimeters) were presented. Figure 14 shows the measurement of $\sigma(\gamma\gamma \to hadrons)$ as a function of $W_{\gamma\gamma}$ compared to a Donnachie and Landshoff type fit $(\sigma_{tot} = As^{\epsilon} + Bs^{-\eta})$ for the total cross section. The fit result for the pomeron dependence, $\epsilon = 0.158 \pm 0.006$ (stat) ± 0.028 (syst), is a factor of two higher than the soft pomeron intercept. Fits to the measured $\sigma(\gamma^*\gamma^* \to hadrons)$ cross sections at $\sqrt{s} = 91$, 183 and 189 GeV yield ϵ values equal to 0.28 ± 0.05, 0.40 ± 0.07 and 0.29 ± 0.03 respectively. These values are not in agreement with a leading order BFKL model with $\epsilon \simeq 0.53$ [39].

REFERENCES

1. M. Inuzuka, these proceedings.
2. A. Donnachie and P.V. Landshoff, *Phys. Lett.* **B296** (1992) 227.
3. J–R. Cudell et al., *Soft Pomeron Intercept*, hep–ph/9712235.
4. C. Royon, these proceedings.
5. H1 Collaboration, C. Adloff et al., *Z. Phys.* **C76** (1997) 613.
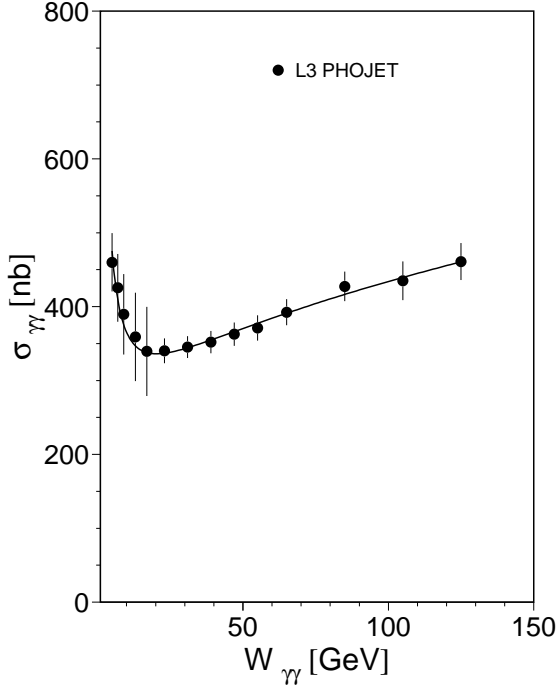6. Yu. L. Dokshitzer, *Sov. Phys. JETP* **46**

Figure 14. The L3 measurement of $\sigma_{\gamma\gamma}$ as a function of $W_{\gamma\gamma}$. The data were corrected for acceptance and efficiency effects using the PHOJET [38] Monte Carlo. The solid line shows the result of a Donnachie and Landshoff type fit for the total cross section.

(1977) 641; V. N. Gribov, L. N. Lipatov, *Sov. J. Nucl. Phys.* **15** (1972) 438; G. Altarelli and G. Parisi, *Nucl. Phys.* **B126** (1977) 298.

7. F.P. Schilling, these proceedings. See also H1 Collaboration, C. Adloff et al., *Eur. Phys. J.* **C6** (1999) 421.
8. P. Bruni and G. Ingelman, *Proceedings of the Europhysics Conference, Marseilles, France*, July 1993, 595.
9. H. Jung, *Comp. Phys. Comm.* **86** (1995) 147.
10. S. Hengstmann, these proceedings.
11. J. Cole, these proceedings.
12. W. Buchmüller, A Hebecker and M.F. McDermott, *Phys. Lett.* **B404** (1997) 353.
13. M. G. Ryskin, *Sov. J. Nucl. Phys.*, 52 (1990) 529.
14. L. Alvero et al., *Tests of Factorization in Diffractive Charm Production and Double Pomeron Exchange*, hep–ph/9805268.
15. G. Ingelman et al., *Comp. Phys. Comm.*, **101** (1997) 135.
16. M. Khakzad, these proceedings.
17. M. Kapichine, these proceedings. See also H1 Collaboration, C. Adloff et al., *Eur. Phys. J.* **C6** (1999) 587.
18. I. Gialas, these proceedings.
19. L. Lönnblad, *Comp. Phys. Comm.* **71** (1992) 15.
20. G. Ingelman, A. Edin and J. Rathsman, *Comp. Phys. Comm.* **101** (1997) 108.
21. T.T Chou and C. N. Yang, *Phys. Rev.* **D50** (1994) 590.
22. P. Markun, these proceedings.
23. B. Cox, these proceedings.
24. A. H. Mueller and W. K. Tang, *Phys. Lett.* **B284** (1992) 123.
25. G. Marchesini et al., *Comp. Phys. Comm.* **67** (1992) 465.
26. B. Clerbaux, these proceedings. See also H1 collaboration, C. Adloff et al., hep–ex/9902019.
27. A. Droutskoi, these proceedings.
28. A. Savin, these proceedings.
29. J. Crittenden, these proceedings.
30. I.F. Ginzburg and D.Yu. Ivanov, *Phys. Rev.* **D54** (1996) 5523.
31. S. J. Brodsky et al., *Phys. Lett.* **B449** (1999) 306.
32. P. Merkel, these proceedings. See also H1 collaboration, C. Adloff et al., hep–ex/9903008.
33. A. Borissov, these proceedings. See also HERMES collaboration, K. Ackerstaff et al., *Phys. Rev. Lett.* **82** (1999) 3025.
34. K. Borras, these proceedings.
35. K. Goulianos, *Phys. Lett.* **B358** (1995) 379.
36. K. Mauritz, these proceedings.
37. H. Vogt, these proceedings. See also L3 Collaboration, M. Acciarri et al., *Phys. Lett.* **B408** (1997) 450.
38. R. Engel and J. Ranft, *Phys. Rev.* **D54** (1996) 4244.
39. S.J. Brodsky, F. Hautmann and D.E. Soper, *Phys. Rev.* **D56** (1997) 6957.